Reaction of HO with Glycolaldehyde, $HOCH_2CHO$: Rate Coefficients (240−362 K) and Mechanism

Rosalin Karunanandan, Dirk Hölscher, Terry J. Dillon, Abraham Horowitz,[#] and John N. Crowley*

Max-Planck-Institut für Chemie, Division of Atmospheric Chemistry, 55020 Mainz, Germany

Luc Vereecken and Jozef Peeters

Katholieke Universiteit Leuven, Division of Quantum Chemistry and Physical Chemistry, Celestijnenlaan 200 F, 3001 Heverlee-Leuven, Belgium

Received: August 2, 2006; In Final Form: November 20, 2006

Absolute rate coefficients for the title reaction, HO + $HOCH_2CHO$ → products (R1), were measured over the temperature range 240−362 K using the technique of pulsed laser photolytic generation of the HO radical coupled to detection by pulsed laser induced fluorescence. Within experimental error, the rate coefficient, k_1, is independent of temperature over the range covered and is given by $k_1(240-362\ \text{K}) = (8.0 \pm 0.8) \times 10^{-12}$ cm^3 molecule^{-1} s^{-1}. The effects of the hydroxy substituent and hydrogen bonding on the rate coefficient are discussed based on theoretical calculations. The present results, which extend the database on the title reaction to a range of temperatures, indicate that R1 is the dominant loss process for $HOCH_2CHO$ throughout the troposphere. As part of this work, the absorption cross-section of $HOCH_2CHO$ at 184.9 nm was determined to be $(3.85 \pm 0.2) \times 10^{-18}$ cm^2 molecule^{-1}, and the quantum yield of HO formation from the photolysis of $HOCH_2CHO$ at 248 nm was found to be $(7.0 \pm 1.5) \times 10^{-2}$.

1. Introduction

Glycolaldehyde, $HOCH_2CHO$, is formed in significant yields during the atmospheric oxidation of the most important biogenically emitted non-methane hydrocarbon, isoprene. As isoprene accounts for about 50% of the total emissions of biogenic species globally,[1] it can have a large impact on several issues of tropospheric chemistry, including the formation of O_3 and the abundance of hydroxyl radicals. $HOCH_2CHO$ is also formed in the HO-initiated oxidation of ethene, where its yield increases significantly with decreasing temperature and amounts to ≈0.7 at upper tropospheric temperatures.[2] $HOCH_2CHO$ has been observed in the planetary boundary layer, where its presence has been associated with biogenic emissions[3] and biomass burning.[4] The observation of high concentrations of short-lived oxidized organic species in the free and upper troposphere[5] implies that an understanding of the low-temperature oxidation of these compounds is important.

In common with other carbonyl compounds, the most important gas-phase atmospheric sinks of $HOCH_2CHO$ are reaction with HO (R1) and/or photolysis (R2), with the HO sink expected to dominate.[6]

$$\text{HO} + \text{HOCH}_2\text{CHO} \rightarrow \text{products} \qquad \text{(R1)}$$

$$\text{HOCH}_2\text{CHO} + h\nu \rightarrow \text{products} \qquad \text{(R2)}$$

The existing kinetic database on the reaction of HO with $HOCH_2CHO$ is however restricted to a set of relative rate measurements at room temperature only,[6−9] which differ by up to a factor of ≈2 in the values of k_1 obtained.[10]

Recent experimental work has shown that the reactions of HO radicals with partially oxidized hydrocarbons such as, for example, acetone[11] or acetaldehyde,[12] can display a complex temperature dependence resulting from competition between direct and indirect abstraction mechanisms. In addition, the rate coefficient for reaction of HO with hydroxy substituted acetone (i.e., $HOCH_2C(O)CH_3$) displays a distinctly different temperature dependence to its non-substituted analogue, which was interpreted in terms of formation and stabilization of pre-reaction complexes.[13]

The present study extends our research in the low-temperature oxidation of partially oxidized organics to explore the temperature dependence of k_1, both experimentally and theoretically, and to gain further insight into the detailed mechanism of reactions of HO with bifunctional species. We also present measurements of the UV absorption spectrum of $HOCH_2CHO$ (210−335 nm, 184.9 nm) and quantum yield data for its photolysis at 248 nm.

2. Experimental Methods

The experimental studies of (R1) were carried out using pulsed laser photolysis (PLP) with pulsed laser induced fluorescence (PLIF) detection of HO. All experiments were conducted under pseudo-first-order conditions, with the concentration of the excess reagent, [$HOCH_2CHO$], determined by on-line optical absorption methods. A schematic diagram of the apparatus is presented in Figure 1.

2.1. UV Cross-Sections and Concentration Measurements of $HOCH_2CHO$. Absorption cross-sections of $HOCH_2CHO$ were determined in three types of experiments. In the first, the

* To whom correspondence should be addressed. E-mail: crowley@mpch-mainz.mpg.de.

[#] Permanent address: Soreq Research Center, Yavne 81800, Israel.

10.1021/jp0649504 CCC: $37.00 © 2007 American Chemical Society
Published on Web 01/12/2007

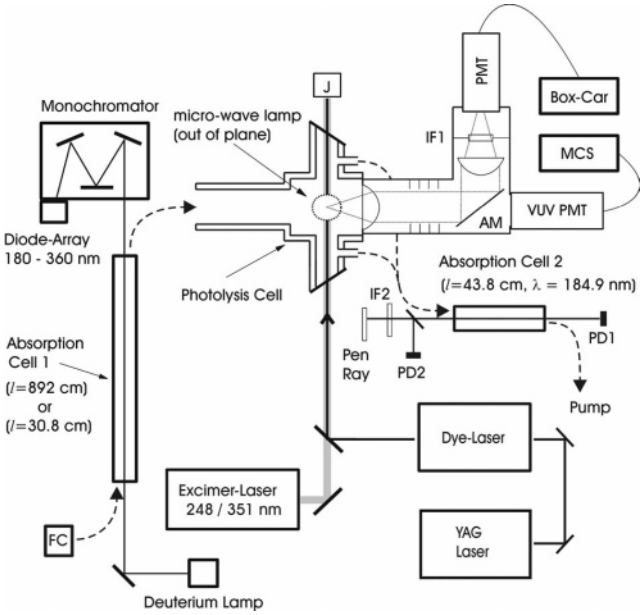

Figure 1. PLP-PLIF/RF experimental setup. J, Joule-meter; PMT, photomultiplier; Box-Car, Box-Car charge integrator; MCS, multichannel scaler; AM, aluminum mirror (movable), FC, flow controllers; Pen Ray, low-pressure Hg Pen-Ray lamp. IF1/2, 309 and 184.9 nm interference filter, respectively; PD1 and PD2, photodiodes. Dashed lines indicate direction of gas flow.

absorption spectrum between 210 and 335 nm was measured using a 30.4-cm-long Pyrex absorption cell fitted with heated quartz windows (360 K). The collimated output from a deuterium lamp provided analysis light that transversed the absorption cell before being focused onto the entrance slit of a 0.5 m monochromator (B&M Spektronik BM50, equipped with a 300 lines/mm grating blazed at 300 nm) and dispersed onto a diode-array detector (Oriel INSTAspec 2). The wavelength-dependent attenuation of radiation by undiluted, static samples of $HOCH_2CHO$ was measured, and [$HOCH_2CHO$] was calculated from its pressure (10 Torr capacitance manometer). The wavelength-dependent cross-sections were calculated from the Beer−Lambert law:

$$\sigma_\lambda = OD_\lambda/[HOCH_2CHO]l \qquad \text{(i)}$$

where l is the optical path length (30.4 cm) and OD_λ is the optical density, defined as $OD_\lambda = \ln(I_{0(\lambda)}/I_{(\lambda)})$. I_0 and I are the transmitted light intensities in the absence and in the presence of $HOCH_2CHO$, respectively.

A second set of experiments using static $HOCH_2CHO$ samples was carried out using the same optical absorption cell but using the 184.9 nm line from a low-pressure Hg lamp as analysis light. In these experiments, the monochromator was purged with N_2 to allow efficient transmission of the 184.9 nm light, which was detected by ≈20 adjacent pixels of the diode array (a result of low instrumental resolution). Cross-sections were calculated as described above.

In a third set of experiments, $\sigma_{184.9nm}$ was determined in a flowing system, with the $HOCH_2CHO$ diluted in N_2. In these experiments, the gas flow first passed through a 892 cm, multipass absorption cell equipped with a deuterium lamp and the monochromator/detector described above to simultaneously detect light intensity at wavelengths between ≈210 and 325 nm. This enabled the concentration of $HOCH_2CHO$ to be derived by comparison to the complete reference absorption spectrum, measured, for example, as described above. The whole gas flow then passed through a 43.8 cm Pyrex absorption cell (downstream of the reaction cell, see Figure 1) where extinction at 184.9 nm was measured using a low-pressure Hg lamp as analysis light source and a 184.9 nm interference filter (fwhm = 5 nm) to remove longer wavelength emissions. In this setup, two photodiodes (one measuring transmitted light, one as reference) were used to monitor absorbance at 184.9 nm. A small correction was made for the presence of stray light at 253.7 nm (≈8% of the intensity of the 184.9 nm line) that transmitted the interference filter. Additional small corrections were made for molecular density changes due to the difference in pressure (usually less than 1%) and temperature between the cells.

2.2. PLP-PLIF Technique. Details of this setup have been published previously,[11] and only a brief description is given here. The experiments were carried out in a jacketed reactor of volume ≈ 500 cm^3 (see Figure 1), which was thermostatted to the desired temperature by circulating a cryogenic fluid through the outer jacket. The pressure in the cell, monitored with 10, 100, and 1000 Torr capacitance manometers, was typically held constant at 60 or 250 Torr, using He or N_2 as bath gas. Gas flow rates, regulated using calibrated mass flow controllers, were between 400 and 2700 cm^3 (STP) min^{-1} (sccm), which ensured that a fresh gas sample was available for photolysis at each laser pulse and prevented a buildup of products.

Fluorescence from HO was detected by a photomultiplier tube (PMT) screened by a 309 nm interference filter and a BG 26 glass cut off filter following excitation of the $A^2\Sigma$ ($v = 1$) ← $X^2\Pi$ ($v = 0$), Q_{11} (1) transition at 281.997 nm. The detection limit in the absence of $HOCH_2CHO$ was found to be ≈10^9 cm^{-3} for a $S/N = 1$ (20 scans)

2.3. Generation of HO Radicals. When conducting absolute rate constant studies of HO reactions, it is always good practice to use more than one source of the radical, so that systematic errors associated with, for example, secondary reactions of the radical precursors can be identified. In the present experiments, HO decay profiles often displayed unexpected kinetic behavior, which led us to use a total of three different generation schemes. These were the photolysis of H_2O_2 at 248 nm (R3), the photolysis of O_3 in the presence of CH_4 (R4−R6), and the photolysis of $HOCH_2CHO$ itself (R7).

$$H_2O_2 + h\nu\ (248\ nm) \rightarrow 2\ HO \qquad \text{(R3)}$$

$$O_3 + h\nu\ (248\ nm) \rightarrow O(^1D) + O_2 \qquad \text{(R4)}$$

$$O(^1D) + CH_4 \rightarrow HO(X^2\Pi, v > 0) + CH_3 \qquad \text{(R5a)}$$

$$\rightarrow H + CH_3O \qquad \text{(R5b)}$$

$$HO(X^2\Pi, v > 0) + CH_4 \rightarrow HO(X^2\Pi, v = 0) + CH_4 \qquad \text{(R6)}$$

$$HOCH_2CHO + h\nu\ (248\ nm) \rightarrow HO + CH_2CHO \qquad \text{(R7)}$$

These schemes and the limitations/potential complications associated with each one are described in detail in section 3.2.

In previous experiments, for example, in studies of the reactions of HO with acetone,[11] we used the 351 nm photolysis of HONO as HO source.

$$HONO + h\nu\ (351\ nm) \rightarrow HO + NO \qquad \text{(R8)}$$

However, the HONO source contains some NO_2 impurity, and $O(^3P)$ generation from the 351 nm dissociation of NO_2 is an unavoidable byproduct of this method of HO production.

Exploratory experiments using this source showed significant HO generation via the reaction of $O(^3P)$ with $HOCH_2CHO$, which, by analogy to CH_3CHO, is expected to have a rate coefficient of $\approx 5 \times 10^{-13}$ cm^3 molecule^{-1} s^{-1} at room temperature.[14] For this reason, we do not report values of k_1 obtained using this source.

2.4 Chemicals. $HOCH_2CHO$ was obtained by gently heating its crystalline dimer (Aldrich) to ≈30−60 °C using a water bath. The gas phase above the crystals was either stored as a pure or diluted sample in pre-evacuated, darkened Pyrex bulbs or eluted into the reactor in a flow of He or N_2, whereby its concentration was varied by slight variation of the water-bath temperature. H_2O_2 (Peroxid-Chemie GmbH, ≈80 wt%) was concentrated to >90 wt% by pumping away water. D_2O_2/H_2O_2 mixtures were obtained by mixing D_2O with concentrated H_2O_2 and then repeating the pumping process. Anhydrous HNO_3 was prepared by distillation of mixtures H_2SO_4 (>90 wt%) with KNO_3. N_2, He, and O_2 (all Messer 5.0, 99.999%), CH_4 (Messer, 99.995%) were used without further purification.

3. Results and Discussion

3.1. Absorption Cross-Sections for $HOCH_2CHO$. Pure $HOCH_2CHO$ samples were prepared by heating its thoroughly degassed dimer and allowing the monomer thus formed to expand directly into a pre-evacuated 5 L bulb until a pressure of 0.5−0.6 Torr was reached. Subsequently, this bulb was conditioned by allowing it to stand for at least 30 min. Then, prior to the optical measurement, it was evacuated and filled again to ~0.4 Torr. $HOCH_2CHO$ was dosed into the optical cell (l = 30.4 cm), and values of I and I_0 were recorded for eight pressures between 0.0805 and 0.355 Torr. The absorption spectrum between ≈210 and 335 nm, calculated using eq (i), is displayed in Figure 2A where it is compared to previous determinations from this and other laboratories. There is clearly very good agreement with the two spectra reported by Magneron et al.,[9] which were obtained in two distinct experimental set-ups and using different $HOCH_2CHO$ samples. At 282 nm, close to the maximum absorption, an unweighted, least-squares fit of the data at this wavelength yields a cross-section of $(6.94 \pm 0.10) \times 10^{-20}$ cm^2 molecule^{-1}, where the errors are 2σ statistical. This value is in excellent agreement with the values of 6.93×10^{-20} and 6.99×10^{-20} cm^2 molecule^{-1}, reported in Magneron et al.,[9] but is higher by about 30% compared to the corresponding value of $(5.37 \pm 0.8) \times 10^{-20}$ cm^2 molecule^{-1} determined by Bacher et al.[6] The errors reported by Bacher et al. are estimated as 15%; Magneron et al. do not report errors close to the absorption maximum. Bacher et al. indicate that, due to the potential presence of H_2O vapor, their measurements may represent a lower limit.

The good agreement with the two results reported in Magneron et al., one of which was obtained in a separate laboratory, and both of which were carried out by different personnel using different experimental set-ups, gives us confidence in the accuracy of our cross-sections.

In a further set of experiments, the cross-section of $HOCH_2CHO$ at 184.9 nm was determined by measuring the extinction of 184.9 nm radiation by pure samples of $HOCH_2CHO$ at pressures between 0.06 and 0.47 Torr. The data are plotted in Figure 2B and display the expected linear relationship between optical density and concentration as defined by eq (i). The cross-section derived from the slope of this plot was $\sigma(184.9\text{ nm}) = (3.85 \pm 0.03) \times 10^{-18}$ cm^2 molecule^{-1}, where the errors are 2σ, statistical only. The low statistical errors reflect precise measurement of the I_0/I ratio by least-squares fitting methods

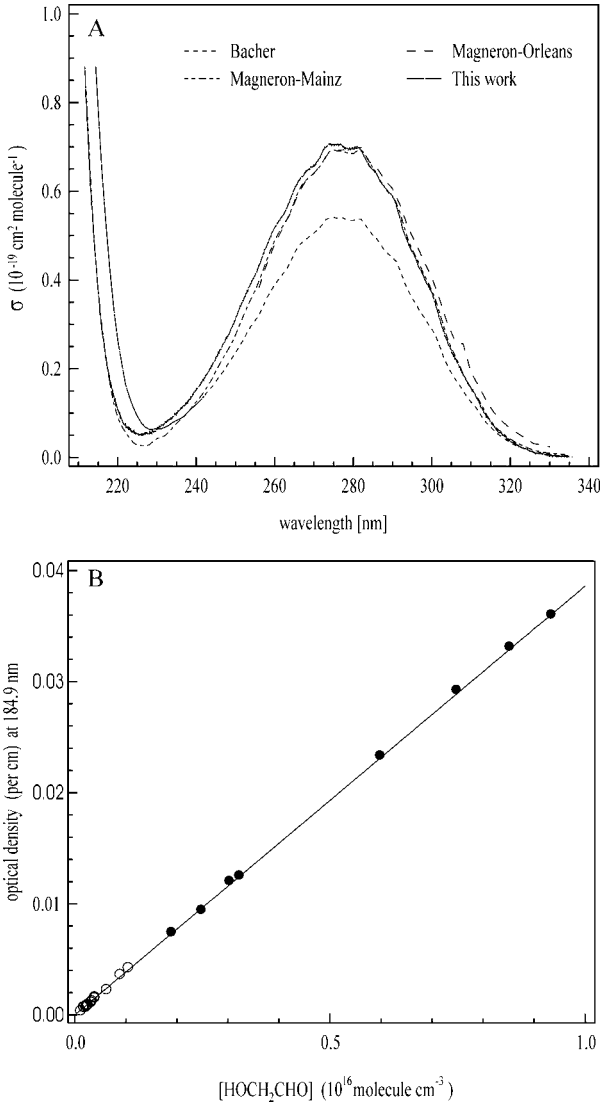

Figure 2. The UV-absorption cross-sections of $HOCH_2CHO$. (A) Diode-array spectrum between ≈210 and 335 nm obtained in this work and by Bacher et al.[6] and Magneron et al.[9] (B) Beer−Lambert plot of optical density at 184.9 nm versus concentration of $HOCH_2CHO$ using direct concentration measurements in static samples (solid circles) and by reference to a diode array spectrum of a flowing mixture (open circles).

and the resulting good linearity of the plot of OD versus concentration. Consideration of possible systematic errors leads us to present a final value of $(3.85 \pm 0.2) \times 10^{-18}$ cm^2 molecule^{-1}.

Having established the cross-section both at 184.9 nm and between 210 and 335 nm, we conducted consistency tests in which a diluted, flowing sample of $HOCH_2CHO$ in N_2 was first passed through the multipass optical cell (l = 892 cm) before flowing into a second optical cell (l = 43.8 nm) in which the optical density at 184.9 nm could be determined on-line (see section 2 for details). The open circles in Figure 2B display the data obtained, whereby the concentration was calculated not from the pressure but from the diode-array spectrum. The good agreement in the two datasets (within combined error limits) provides further support for the accuracy of our absorption spectrum.

In all kinetic experiments (see below), concentrations were determined optically at 184.9 nm using the downstream, single-wavelength system as this allowed $[HOCH_2CHO]$ to be

measured simultaneously with the measurement of an HO decay profile. The value of $\sigma_{184.9nm} = (3.85 \pm 0.2) \times 10^{-18}$ cm^2 molecule^{-1} taken from the direct determination at this wavelength was used to calculate [$HOCH_2CHO$].

3.2. Kinetics of HO + $HOCH_2CHO$. The PLP-PLIF studies were all carried out under pseudo-first-order conditions with [$HOCH_2CHO$] ≫ [HO]. Despite this, in some instances, non monoexponential decays of HO were observed, presumably due to secondary reactions inherent to the scheme of HO generation. We thus present and discuss the data from each of the three HO generation schemes used separately.

3.2.1. Photolysis of H_2O_2 at 248 nm. The photolysis of H_2O_2 at 248 nm (R3) has been routinely used to generate HO radicals in this and other laboratories, though its use is usually limited to temperatures above 250 K due to its low vapor pressure.

$$H_2O_2 + h\nu\ (248\ nm) \rightarrow 2\ HO \qquad (R3)$$

A further limitation encountered in this study was the photolysis of $HOCH_2CHO$ at 248 nm, which has a significant absorption cross-section at this wavelength (see above). HO decay profiles obtained following the photolysis of H_2O_2/$HOCH_2CHO$ mixtures at high laser fluence were not monoexponential but were affected by secondary HO formation from radical fragments (e.g., HCO and CH_2OH) resulting from $HOCH_2CHO$ photolysis. This problem was overcome by working with low laser fluences (typically 1−2 mJ cm^{-2}), which necessitated the use of high H_2O_2 concentrations (≈10^{14} molecule cm^{-3}) to generate sufficient concentrations of the HO radical. The disadvantages associated with working under these conditions are the restriction of the accessible temperature range to $T > 273$ K to avoid condensation of H_2O_2 and an enhanced rate of loss of HO in the absence of $HOCH_2CHO$ owing to its reaction with H_2O_2 ($k_9 \approx 2 \times 10^{-12}$ cm^3 molecule^{-1} s^{-1}).[10]

$$HO + H_2O_2 \rightarrow H_2O + HO_2 \qquad (R9)$$

Representative HO decay traces thus obtained are plotted in Figure 3A, which exemplify the strictly monoexponential decays obtained when suitable conditions were chosen. The decay of HO is then described by

$$[HO]_t = [HO]_0 \exp\{-(k' + d)t\} \qquad (ii)$$

where $[HO]_t$ is the HO concentration (molecules cm^{-3}) at time $= t$ after the excimer laser pulse, k' is the first-order decay coefficient (s^{-1}) and is equal to k_1[$HOCH_2CHO$], and d (s^{-1}) accounts for diffusion of HO out of the reaction zone and reaction of HO with H_2O_2. The slope of plots of k' versus [$HOCH_2CHO$] (see, e.g., Figure 3B) yields the bimolecular rate coefficient, k_1. Data were obtained at several temperatures between 275 and 344 K using this source of HO, with the resulting values of k_1 obtained varying from 7.5 to 8.8 × 10^{-12} cm^3 molecule^{-1} s^{-1}. The results obtained at each temperature are listed in Table 1.

At low fluences, the resulting low HO concentrations and hence low conversion of $HOCH_2CHO$ ensures that secondary loss of HO, for example, with itself or with products can be disregarded fully. This could be confirmed by showing that the variation of the photolysis laser fluence, and thus radical concentrations, by a factor of ≈3 had no measurable influence on the HO decay coefficient.

Experiments were also carried out using the photolysis of D_2O_2 as a source of DO. DO decay profiles (detected by excitation at 286.7 nm) were strictly exponential even at high laser fluence, suggesting that the source of non-monoexponential behavior in the H_2O_2 experiments at high laser fluence was the release of the hydroxyl group from a radical fragment of $HOCH_2CHO$. The DO traces were analyzed as described above for HO, and the rate coefficients obtained at three temperatures between 278 and 337 K are also listed in Table 1.

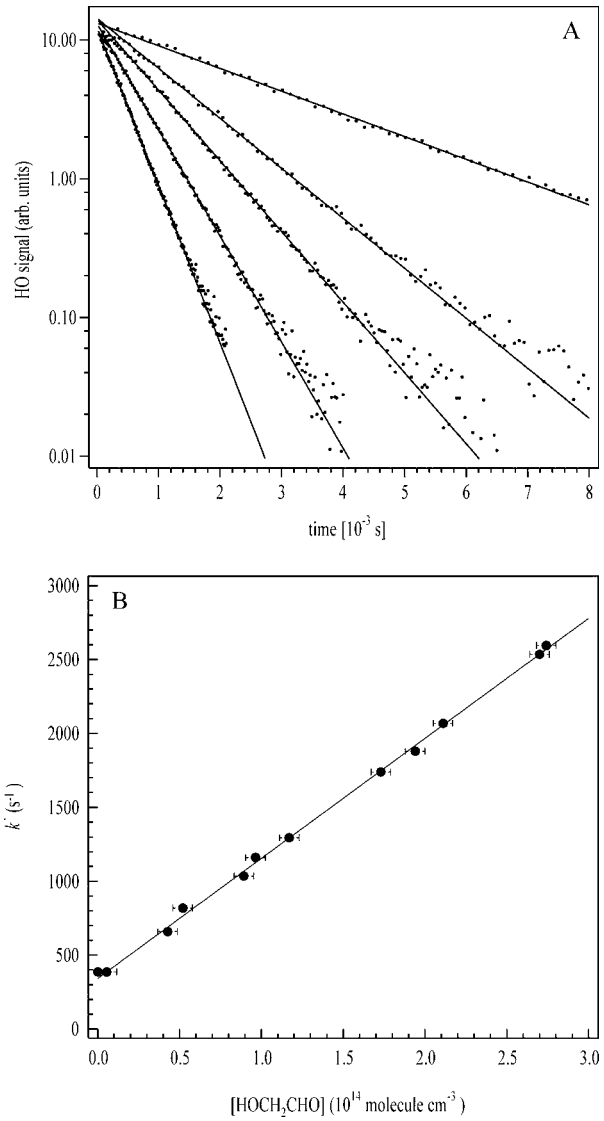

Figure 3. (A) Representative HO decay profiles obtained using the photolysis of H_2O_2 in the presence of varying amounts of $HOCH_2CHO$, illustrating the monoexponential nature of the decay over up to 3 orders of magnitude decrease in signal. The $HOCH_2CHO$ concentrations (in units of 10^{14} molecule cm^{-3}) were 0, 0.56, 1.04, 1.87, and 2.95 (going from the uppermost to lowermost trace). (B) Plot of k' versus [$HOCH_2CHO$], the slope of which yields the bimolecular rate coefficient k_1 according to eq (ii). The error bars on the $HOCH_2CHO$ concentration are statistical (2σ) only and do not take into account errors in the absorption cross-section of $HOCH_2CHO$ at 184.9 nm. Error bars on k' are obscured by the symbols.

3.2.2. 248 nm Photolysis of O_3/CH_4. Reactions (R4−R6), the 248 nm photolysis O_3 in the presence of CH_4 (see section 2), served as an alternative HO generation scheme with He as the bath gas. The role of methane, present at 5−16 × 10^{16} molecule cm^{-3}, is twofold, serving both as scavenger of O(^{1}D) and quencher of vibrationally excited HO (R6). Under the present conditions, the formation of vibrationally relaxed HO is complete within ≈20 μs.[15,16]

The relatively high absorption cross-section of O_3 at 248 nm allowed very low precursor concentrations ([O_3] < 5 × 10^{12}

TABLE 1: Summary of Rate Coefficient Data Obtained in This Work

T(K)	HO (DO) source	k_1[a]
240	$O_3/CH_4 + h\nu$ (248 nm)	8.02 ± 0.19
243	$O_3/CH_4 + h\nu$ (248 nm)	8.06 ± 0.20
245	$HOCH_2CHO + h\nu$ (248 nm)	7.80 ± 0.14
248	$O_3/CH_4 + h\nu$ (248 nm)	8.40 ± 0.16
250	$O_3/CH_4 + h\nu$ (248 nm)	8.01 ± 0.18
253	$O_3/CH_4 + h\nu$ (248 nm)	8.12 ± 0.33
254	$HOCH_2CHO + h\nu$ (248 nm)	8.02 ± 0.68
255	$O_3/CH_4 + h\nu$ (248 nm)	7.89 ± 0.24
258	$O_3/CH_4 + h\nu$ (248 nm)	8.28 ± 0.24
263	$O_3/CH_4 + h\nu$ (248 nm)	8.14 ± 0.18
268	$O_3/CH_4 + h\nu$ (248 nm)	8.26 ± 0.19
274	$O_3/CH_4 + h\nu$ (248 nm)	8.15 ± 0.23
275	$H_2O_2 + h\nu$ (248 nm)	7.59 ± 0.16
278	$D_2O_2 + h\nu$ (248 nm)	8.89 ± 0.23
280	$O_3/CH_4 + h\nu$ (248 nm)	8.04 ± 0.35
280	$H_2O_2 + h\nu$ (248 nm)	8.8 ± 0.7 (N_2, 250 Torr)
289	$O_3/CH_4 + h\nu$ (248 nm)	7.86 ± 0.19
296	$H_2O_2 + h\nu$ (248 nm)	7.54 ± 0.08
296	$O_3/CH_4 + h\nu$ (248 nm)	7.94 ± 0.19
297	$H_2O_2 + h\nu$ (248 nm)	7.91 ± 0.16
297	$D_2O_2 + h\nu$ (248 nm)	8.84 ± 0.20
297	$HOCH_2CHO + h\nu$ (248 nm)	7.89 ± 0.15
298	$H_2O_2 + h\nu$ (248 nm)	7.2 ± 0.5 (N_2, 250 Torr)
299	$H_2O_2 + h\nu$ (248 nm)	8.4 ± 0.7 (N_2, 250 Torr)
298	$H_2O_2 + h\nu$ (248 nm)	7.74 ± 0.13
300	$O_3/CH_4 + h\nu$ (248 nm)	7.58 ± 0.25
304	$O_3/CH_4 + h\nu$ (248 nm)	8.17 ± 0.24
311	$O_3/CH_4 + h\nu$ (248 nm)	8.08 ± 0.25
316	$O_3/CH_4 + h\nu$ (248 nm)	7.69 ± 0.17
324	$H_2O_2 + h\nu$ (248 nm)	7.92 ± 0.05
324	$O_3/CH_4 + h\nu$ (248 nm)	7.59 ± 0.19
332	$O_3/CH_4 + h\nu$ (248 nm)	7.69 ± 0.14
337	$D_2O_2 + h\nu$ (248 nm)	8.68 ± 0.17
338	$HOCH_2CHO + h\nu$ (248 nm)	7.74 ± 0.19
338	$O_3/CH_4 + h\nu$ (248 nm)	8.46 ± 0.28
338	$H_2O_2 + h\nu$ (248 nm)	8.4 ± 0.7 (N_2, 250 Torr)
339	$H_2O_2 + h\nu$ (248 nm)	8.32 ± 0.14
343	$O_3/CH_4 + h\nu$ (248 nm)	8.03 ± 0.31
344	$H_2O_2 + h\nu$ (248 nm)	8.32 ± 0.09
352	$O_3/CH_4 + h\nu$ (248 nm)	8.07 ± 0.21
362	$O_3/CH_4 + h\nu$ (248 nm)	8.11 ± 0.19

[a] Units of 10^{-12} cm^3 molecule^{-1} s^{-1}. The errors account for statistical errors (2σ) both in determination of k' and in the concentration of $HOCH_2CHO$. They do not contain systematic errors in, for example, the determination of the $HOCH_2CHO$ concentration caused by error in its cross-section. The errors reported for rate coefficients derived using k'_{init} (O_3/CH_4 experiments) are not rigorously propagated due to coupling of the *A* and *B* terms (see text for details). The errors reported for the experiments carried out in N_2 are larger due to more noisy HO signals. Except where indicated, the experiments were carried out using 60 Torr He as bath gas.

molecule cm^{-3}) and low laser fluences to be employed and hence minimized any undesired secondary chemistry resulting from $HOCH_2CHO$ photolysis. Furthermore, the reagents O_3 and CH_4 have sufficiently high vapor pressures to enable HO generation at low temperatures and react rather slowly with HO, especially at low temperatures with $k(HO + O_3) \approx 3 \times 10^{-14}$ cm^3 molecule^{-1} s^{-1} and $k(HO + CH_4) \approx 1 \times 10^{-15}$ cm^3 molecule^{-1} s^{-1} at 230 K.[10] Representative HO decay profiles using this scheme are displayed in Figure 4A. In contrast to those obtained using H_2O_2 photolysis, the decays were frequently (but not always) biexponential, with indications of secondary HO formation at long reaction times. A plausible explanation of this behavior is the reaction of H atoms, formed in a minor channel (20%)[10] of reaction R5, with O_3:

$$H + O_3 \rightarrow HO + O_2 \qquad \text{(R10)}$$

O_3 concentrations of $\approx 10^{12}$ molecule cm^{-3} and a rate coefficient

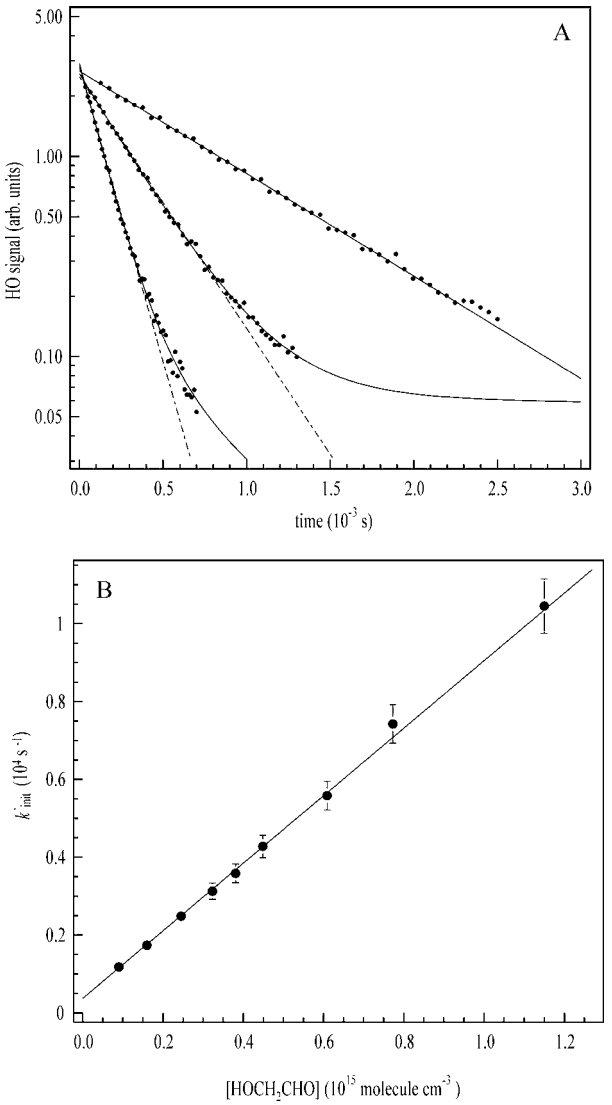

Figure 4. (A) Representative HO decay profiles obtained using the 248 nm photolysis of O_3/CH_4 in the presence of varying amounts of $HOCH_2CHO$. The dotted lines are monoexponential fits to the data according to eq (ii). The solid lines are biexponential fits according to eq (iii). The $HOCH_2CHO$ concentrations (in units of 10^{14} molecule cm^{-3}) were 0.97, 3.48, and 8.33 (going from the uppermost to lowermost trace). (B) Plot of k'_{init} (see text for derivation) versus [$HOCH_2CHO$], the slope of which yields the bimolecular rate coefficient k_1 according to eq (ii). Statistical error bars on the $HOCH_2CHO$ concentration are obscured by the symbols. The error bars on k' are estimates as rigorous propagation of errors in k'_{init} is not possible if the two exponential terms are coupled.

of $k_{10} = 1.5 \times 10^{-10}$ cm^3 molecule^{-1} s^{-1} [10] result in HO production rates of >200 s^{-1}, which may be compared to measured decay constants of between 500 and 5000 s^{-1}. An aditional, potential source of H atoms is the reaction of CH_3 with O_3 to form $CH_3O + O_2$, and subsequent decomposition of "hot" CH_3O to HCHO and H. The factor of ≈10 lower rate coefficient for $CH_3 + O_3$ compared to $H + O_3$ and quenching of hot CH_3O will however probably make this reaction insignificant.

In previous experiments examining the kinetics of HO with alcohols using the same HO source,[17] this undesired OH generation was not encountered as much higher laser fluences were used, resulting in complete removal of O_3 during the laser pulse. In those experiments, use of high fluences was possible because, in contrast to $HOCH_2CHO$, the alcohols do not absorb light at 248 nm. The observation that monoexponential decays

were (sometimes) observed at high temperatures may be due to scavenging of the H atom by $HOCH_2CHO$, which is expected to have a large barrier and become sufficiently efficient to compete with $H + O_3$ only at high T.

Since the kinetics of this secondary HO source is also pseudo-first-order ($[O_3] \gg [H]$), expression (iii) may be fit to the data:

$$[HO]_t = A \exp(-Bt) + C \exp(-Dt) \qquad \text{(iii)}$$

where $A = [HO]_0 - C$, $B = k' + d$, $C = [H]_0\{k'_{10}/(k_a - k_b)\}$, $D = k_{10}[O_3] + d'$ and k_a and k_b are equal to $k' + d$ and $k'_{10} + d'$ (the first-order coefficient for H atom diffusion), respectively. This expression always fit each dataset well, yet due to experimental noise and coupling with the other exponential term at low $[HOCH_2CHO]$, the desired parameter, k', could not be independently extracted. This is compounded by the fact that reactions (R5) and (R6) are completed shortly (1−2 μs) after time-zero. For these reasons, we have extracted the initial decay constant, k'_{init}, via (iv).

$$k'_{init} \approx k' + d = (AB + CD)/(A + C) \qquad \text{(iv)}$$

This is a valid approximation provided that the loss rate of OH is much larger than the production rate, i.e., $k' \gg k'_{10}$ and $[OH]_0 > [H]_0$. As the initial HO decays were close to exponential over a large proportion of their decay (see Figure 4A), this condition is clearly fulfilled. The solid lines in Figure 4A show the fits to the biexponential expression (iii), while the dotted lines indicate the result if the simpler, monoexponential expression (ii) is used. Expression (ii) often systematically underestimated k' though the exact correction factor, presumably dependent on the concentration of O_3, varied from 0 to 10%. A plot of k'_{init} versus $[HOCH_2CHO]$ is given in Figure 4B, and all data obtained using this HO source are listed in Table 1. The rate coefficients thus obtained (240−362 K) are seen to be in good agreement with those obtained using the H_2O_2 source (in the common temperature regime) and the simpler kinetic analysis, providing justification of this procedure. Variation of the laser fluence over a large range had no significant effect on values of k'_{init} obtained.

3.2.3. Photolysis of $HOCH_2CHO$ at 248 nm. A third source of HO utilized in these experiments was the direct photolysis of $HOCH_2CHO$ at 248 nm, which has a minor channel forming HO and (presumably) CH_2CHO (R7). Monoexponential HO decays could be obtained using this source only if low laser fluences were used, as exemplified by the lower HO trace in Figure 5A. Because of the relatively low HO concentrations obtained, the signal was rather more noisy than those obtained using the other HO sources described above. As the laser fluence was increased, the HO concentration scaled accordingly, but the decays became progressively biexponential as shown by the upper HO trace in Figure 5A. The cause of the apparent secondary HO formation is clearly related to the presence of high concentrations of radical fragments from $HOCH_2CHO$ photolysis, which is expected to generate, for example, HCO, $HOCH_2$, and CH_2CHO (see section 3.4). Similar effects could be obtained by keeping the laser fluence constant, but varying the concentration of $HOCH_2CHO$, whereby monoexponential HO decays were obtained at low $HOCH_2CHO$ only. The reactions of thermalized radicals such HCO, $HOCH_2$, and CH_2CHO among themselves are expected to lead to stable products such as CO, HCHO, CH_3OH, diols and dicarbonyls, but pathways to HO are not obvious and may involve nonthermalized species. In this context, we note that a 248 nm photon has

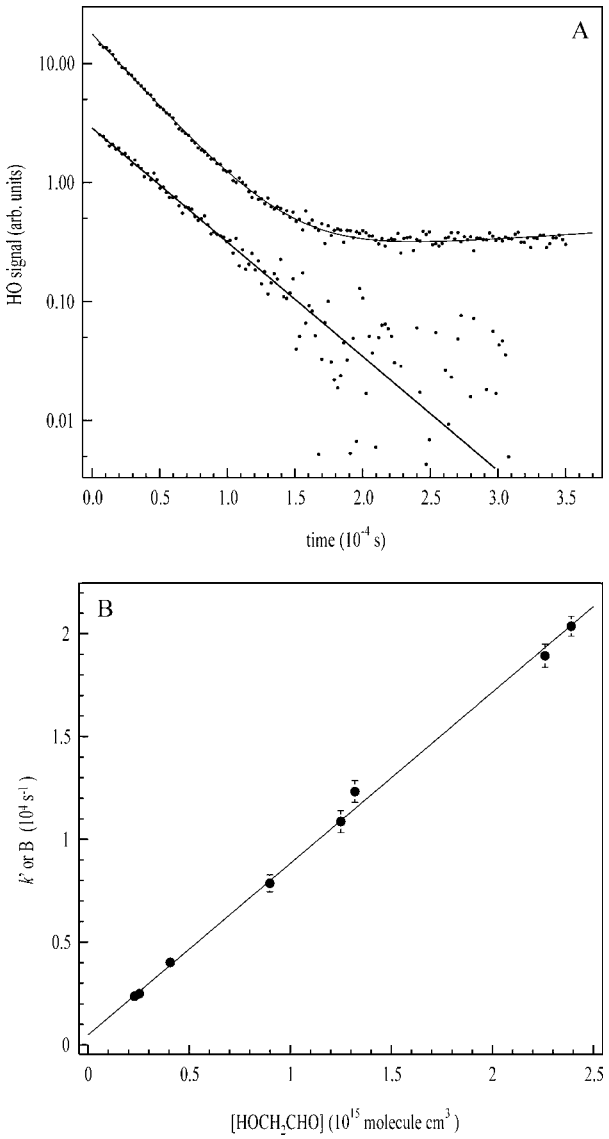

Figure 5. (A) Representative HO decay profiles obtained using the 248 nm photolysis of $HOCH_2CHO$ as HO source. The lower decay trace was obtained at a laser fluence of 26 mJ cm^{-2} and a $HOCH_2CHO$ concentration of 2.73×10^{14} molecule cm^{-3} and is fit to eq (ii). The upper HO trace was obtained at a factor of ≈10 higher laser fluence and $[HOCH_2CHO] = 3.48 \times 10^{14}$ molecule cm^{-3} and is fit to a biexponential expression (iii). Error bars on k' are statistical (2σ); statistical error bars on the $HOCH_2CHO$ concentration are obscured by the symbols.

≈140 kJ mol^{-1} energy in excess of that needed to form HCO and $HOCH_2$ from $HOCH_2CHO$.

As the experimental procedure for determining the rate coefficient involves variation of $[HOCH_2CHO]$, individual HO decay profiles were fit to either equation (ii) or (iii) depending on whether the HO profile was mono- or biexponential.

In contrast to those experiments described above, in which O_3 was photolyzed in the presence of CH_4, the photolysis of $HOCH_2CHO$ produces HO instantaneously (within the laser pulse duration of ≈20 ns) and biexponential decays obtained using $HOCH_2CHO$ photolysis could be analyzed to give sufficiently decoupled parameters B and D. As the majority of the experiments were conducted at low fluence, perturbations from monoexponential decays were observed only at long reaction times, and values of k' obtained from monoexponential fits to the data were generally only between 0 and 5% lower than the parameter B (or D) from the biexponential fits. The

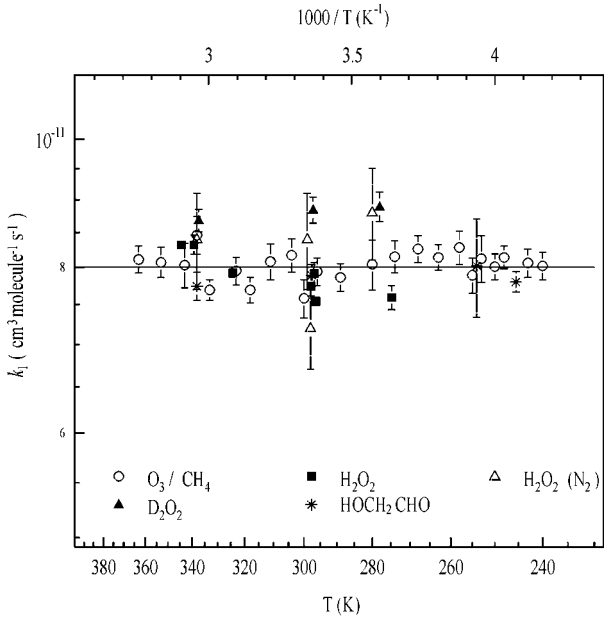

Figure 6. Arrhenius plot of all data obtained in the present study identifying the different schemes to generate HO and DO (solid triangles). Over the temperature range covered and within the experimental scatter of this study, the rate coefficient is independent of temperature and is described by the solid line at $k_1 = 8.0 \times 10^{-12}$ cm^3 molecule^{-1} s^{-1}.

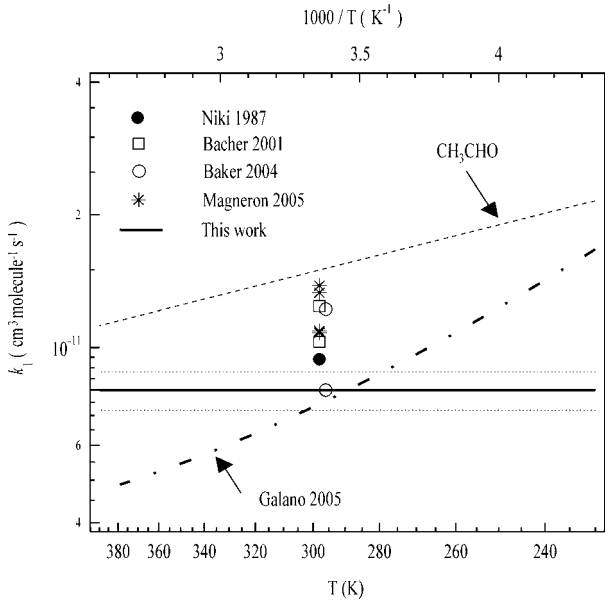

Figure 7. Comparison of the present dataset with relative rate coefficients at room temperature. The error bars on the relative rate data are not shown for the sake of clarity. The dotted lines above and below the present result indicate overall uncertainty (2σ). The rate coefficients obtained in units of 10^{-12} cm^3 molecule^{-1} s^{-1} (corrected for updates in the rate coefficients for HO with the reference compound) and as reported recently by IUPAC[10] are as follows. Niki 1987:[7] $k_1 =$ (9.40 ± 0.90) relative to acetaldehyde; Bacher 2001:[6] $k_1 =$ (12.4 ± 1.6) relative to acetaldehyde, $k_1 =$ (10.3 ± 0.7) relative to propene; Baker 2004:[8] $k_1 =$ (12.20 ± 2.0) relative to 1,2-butanediol, $k_1 =$ (8.0 ± 1.7) relative to 2-methyl-3-butene-2-ol; Magneron 2005:[9] $k_1 =$ (10.8 ± 0.8) relative to diisopropyl ether, $k_1 =$ (13.3 ± 1.5) relative to diethyl ether, $k_1 =$ (10.9 ± 0.9) relative to 1,3-dioxolane, $k_1 =$ (13.8 ± 1.7) relative to acetaldehyde. For comparison, we also show the theoretical result of Galano[22] and the temperature dependence of the rate coefficient for reaction of HO with CH_3CHO.[12]

dependence of either B or D on the concentration of $HOCH_2CHO$ was inspected and seen to vary linearly with [$HOCH_2CHO$]. Either this parameter (or k') was plotted versus [$HOCH_2CHO$] to obtain k_1 as shown in Figure 5B. The rate coefficients obtained by this method between 245 and 338 K are listed in Table 1.

Within experimental uncertainty, the measured rate coefficients were found to be independent of the variation of the laser fluence (see above), any of three HO generation schemes and bath gas pressure ($60 < p$/Torr < 250) and its identity (He or N_2) and indeed, independent of temperature. The lack of a temperature dependence is illustrated in Figure 6 where the complete dataset is plotted in Arrhenius format, $k(T) = A \exp(-E/T)$. Over the temperature range studied, the rate coefficient (units of cm^3 molecule^{-1} s^{-1}) is given by $k_1(240-362\ \text{K}) = (8.0 \pm 0.8) \times 10^{-12}$ cm^3 molecule^{-1} s^{-1} where the uncertainty contains an estimate for systematic errors, predominantly the error in $\sigma_{184.9\text{nm}}$, which directly impacts the values obtained. Figure 6 also displays rate coefficients for the reaction of DO with $HOCH_2CHO$, which are consistently higher (by ≈10%) than those for HO, with data at 278, 297, and 337 K indicating an essentially temperature-independent rate coefficient of $\approx 8.8 \times 10^{-12}$ cm^3 molecule^{-1} s^{-1}. A slightly higher value for the rate coefficient of DO with organics is consistent with measurements with reactions of HO with, for example, CH_3OH,[17] methane,[18] and butane,[19] where the 5−10% enhancement in rate coefficient are related to shifts in zero point energies of transition states.[18] Importantly, the DO data serve to confirm the independence of k_1 on temperature and also rule out the possibility that we are underestimating the true rate coefficient due to rapid regeneration of HO radicals from, for example, decomposition of radical fragments containing the C−OH entity.

In the present work, accurate kinetic data on the reaction of HO with $HOCH_2CHO$ have been obtained over a range of temperatures for the first time. We now compare our results to the previous, relative measurements of the rate coefficient at room temperature, which are plotted along with the present data in Figure 7. The caption to Figure 7 includes the complete set of literature values of k_1. Immediately apparent from this figure is the large scatter in the relative rate measurements which reveal differences of a factor of ≈2. Some of this scatter is certainly related to the use of a total of seven different reference compounds, for some of which the rate coefficients with HO are probably insufficiently accurately known. On the other hand, three studies have derived k_1 relative to $k(\text{HO} + CH_3CHO)$ yet return values of $k_1/k(\text{HO} + CH_3CHO)$ that vary between 0.63 ± 0.06 (Niki et al.[7]), 1.03 ± 0.13 (Bacher et al.[6]), and 0.92 ± 0.11 (Magneron et al.[9]). Such scatter in the relative rate measurements is a strong indication that secondary reactions that form or remove $HOCH_2CHO$ or the reference compound, or which result in detection interferences may play a role. In this context, we note that Bacher et al. made large adjustments to their relative decay rates (≈20%) to take into account the effects of photolysis and wall loss of $HOCH_2CHO$ in their studies and increased the errors on their rate coefficient (1.1 ± 0.3) $\times 10^{-11}$ cm^3 molecule^{-1} s^{-1} to reflect this uncertainty.

Relative rate measurements can have advantages over absolute methods (such as, for example, PLP-PLIF) if the reactants are difficult to obtain as pure samples. The presence of reactive impurities can then result in absolute rate coefficients that are too high, especially if the rate coefficient investigated is small. As the present dataset returns one of the lowest values of k_1 measured to date, this is clearly not the case. The determination of the concentration of the excess reagent is frequently the main source of error in absolute (or direct) kinetic studies carried out under pseudo-first-order conditions. The present experiments

utilized in-situ absorption spectroscopy to determine the concentration of $HOCH_2CHO$ and thus required accurate absorption cross-sections. As described in section 3.1, the good agreement between our spectrum and those measured in other laboratories strongly implies that our concentration is known to better than 10% and cannot be the reason for the low values of the rate coefficients obtained. In this context, we note that use of the cross-sections of Bacher et al.,[6] the only case where the literature cross-sections disagree, would *reduce* our rate coefficients further by ≈30%.

We may also consider the potential role of dimer formation by $HOCH_2CHO$ as a route to deriving a rate coefficient that is too low. Our observations that dilute gas-phase $HOCH_2CHO$ samples are stable for several hours at low pressures (e.g., less than one Torr) is confirmed by the literature,[6,7] implying that re-dimerization of monomeric $HOCH_2CHO$ at low pressures at room temperature is not significant. This may be seen in Figure 2B, which displays a perfectly linear plot of optical density at 184.9 nm versus $HOCH_2CHO$ concentration. As the monomer/dimer ratio is quadratic in $[HOCH_2CHO]$, evidence of dimer formation would be provided by a reduction in the slope of this plot at high $[HOCH_2CHO]$, which is clearly not observed. We must however also recall that, whereas our optical measurements of $[HOCH_2CHO]$ are always conducted at room temperature, the reaction vessel can be as cool as 240 K, which would favor dimerization. In this case, the linear plot of k' versus $[HOCH_2CHO]$ at low temperatures provides strong evidence against a substantial fraction of $HOCH_2CHO$ being in the form of dimers. We are unaware of an equilibrium coefficient for dimerization of $HOCH_2CHO$ to help confirm our qualitative observations.

Having failed to identify a likely source of systematic error in our studies that would result in determination of a rate coefficient that is too low, we turn to the relative rate measurements. As mentioned above, the large scatter in the relative rate measurements is a strong indication of secondary reactions that form or remove $HOCH_2CHO$ or the reference compound. Both Bacher et al.[6] and Magneron et al.,[9] using metal or glass reactors, correct their data for unknown "dark" reactions that remove significant amounts of $HOCH_2CHO$ on the timescale of their experiments, which are typically on the order of hours. On the other hand, Baker et al.[8] report negligible wall loss rates in their Teflon reactor. Although the relative rate data are generally corrected for wall loss, this correction factor is usually determined in experiments without light and may be a lower limit to the true wall loss if the wall reactivity is enhanced by the presence of UV-light or by products of photochemistry that adsorb to the wall. In this respect, the relative rate studies of Bacher et al. and Magneron et al. report carbon balances significantly less than unity. In contrast, the present experiments, in which decays of HO are measured over a few milliseconds, are essentially wall free, and such effects can be ruled out.

A further, major difference between the relative rate measurements and the present direct study is the bath gas identity and pressure. Whereas all of the relative rate measurements were conducted at 1 atm pressure of air, the present rate coefficient was obtained at pressures of 60 Torr in He or 250 Torr N_2 bath gas.

The thermal dissociation (to form HO) of the initially formed radical product of R1 (e.g., $HOCH_2CO$ or HOCHCHO would result in an underestimation of k_1 in the present experiments if it were sufficiently rapid. The presence of O_2 in the relative measurements would reduce or remove this effect by scavenging these radicals before they could dissociate back to HO. Theoretical work[20] has shown that the $HOCH_2CO$ radical may decompose to $CO + CH_2OH$ with a rate coefficient of 30000 s^{-1} in air at one atmosphere pressure at 298 K. This translates to a lifetime of ≈1 ms for $HOCH_2CO$ in our experiments at 60 Torr He, assuming the decomposition is already in its low-pressure regime at one atmosphere. The alternate decomposition channel to form $HO + CH_2CO$ is endothermal by at least 120 kJ/mol and therefore not thermodynamically feasible. No accurate information is available on the thermal stability of the other possible organic radicals, HOCHCHO and OCH_2CHO, though it is hard to envisage that a decomposition channel may exist that releases HO radicals, as even the thermochemically most advantageous route $OCH_2CHO \rightarrow HO + CH_2CO$ can be estimated to be endothermal by about 100 kJ/mol. Note also that the good agreement between the rate coefficients obtained with HO and DO confirms that such effects were negligible in our experiments.

Thus, although we cannot rigorously explain the poor agreement between our dataset, and the rather scattered set of room-temperature rate coefficients obtained by relative rate methods, there are indications that the relative rate methods may overestimate k_1. Despite this, we note that our room-temperature result of $(8.0 \pm 0.8) \times 10^{-12}$ cm^3 molecule^{-1} s^{-1} agrees with the value of (8.0 ± 1.7) cm^3 molecule^{-1} s^{-1} of Baker et al.[8] and, within experimental uncertainty, with the values of Niki et al.[7] ($(9.4 \pm 0.9) \times 10^{-12}$ cm^3 molecule^{-1} s^{-1}) and the average number presented by Bacher et al.[6] (page 184 of their manuscript) of $(1.1 \pm 0.3) \times 10^{-11}$ cm^3 molecule^{-1} s^{-1}. The latest IUPAC recommendation, considering all data prior to the present result, lies at k_1 (298 K) = $(1.1 \pm 0.3) \times 10^{-11}$ cm^3 molecule^{-1} s^{-1}.

Figure 7 includes a plot of the rate coefficients for the reaction of HO with CH_3CHO, acetaldehyde, also determined in this laboratory in the same experimental setup. The reaction of HO with CH_3CHO has a larger rate coefficient than k_1 and displays a negative dependence on temperature, which is related to the formation of pre-reaction complexes.[12] In a recent experimental and theoretical study of the reaction of HO with $HOCH_2C(O)CH_3$, we have shown how hydroxy substitution (i.e., comparison with $CH_3C(O)CH_3$) results in a large enhancement of the rate coefficient at all temperatures investigated and broadens the temperature region in which a negative temperature dependence is observed. These observations are the opposite of what we observe for CH_3CHO and $HOCH_2CHO$.

To gain more insight into the reaction of HO with $HOCH_2CHO$ and to explain some of the features of its reactivity described above, a theoretical study of (R1) has been undertaken.

3.3. Theoretical Considerations for HO + $HOCH_2CHO$. *3.3.1. Site-Specific Rate Coefficients.* There are several thermodynamically possible product channels in the reaction of HO with $HOCH_2CHO$:

$$HO + HOCH_2CHO \rightarrow HOCH_2CO\bullet + H_2O \quad \text{(R1a)}$$

$$\rightarrow HOC\bullet HCHO + H_2O \quad \text{(R1b)}$$

$$\rightarrow \bullet OCH_2CHO + H_2O \quad \text{(R1c)}$$

Product studies[7,9,21] have shown that the reaction proceeds mainly (80−85%) via abstraction at the aldehydic C−H bond (R1a), with ≈15−20% abstraction at the CH_2 group (R1b).

The most recent theoretical work,[22] which predicts a negligible contribution <0.5% for channel R1c, concurs with this distribution. The reaction of HO + acetaldehyde, differing only

in the absence of the hydroxy substituent, also proceeds nearly exclusively (95%) by abstraction of the aldehydic H.[23,24]

$$HO + CH_3CHO \rightarrow \text{products} \quad \text{(R11)}$$

$$\rightarrow H_2O + CH_3CO \quad \text{(R11a)}$$

The overall rate coefficient at 298 K for the HO + $HOCH_2$-CHO reaction, 8×10^{-12} cm^3 molecule^{-1} s^{-1} as measured in this study, is lower than for HO + CH_3CHO ($k_{11} = 1.5 \times 10^{-11}$ cm^3 molecule^{-1} s^{-1}).[12] It follows that the lower rate coefficient for glycolaldehyde must be mostly due to a decrease in the abstraction rate of the aldehydic hydrogen compared to acetaldehyde. i.e., $k_{11a} = 0.95 \times 1.5 \times 10^{-11} = 1.4 \times 10^{-11}$ cm^3 molecule^{-1} s^{-1} and $k_{1a} = 0.80 \times 8 \times 10^{-12} = 6.4 \times 10^{-12}$ cm^3 molecule^{-1} s^{-1}.

As the strength of the C−H bond of the abstracted hydrogen correlates well with the rate of abstraction,[25−27] examining the bond strengths in these molecules can elucidate the reasons for the observed difference. The correlation holds provided the product radicals are considered to have no or a similar type of resonance stabilization (e.g., vinoxy stabilization) and when the abstraction reaction enthalpy is not affected by other effects such as significant changes in H-bonding. On the basis of a large number of bond strength calculations combined with experimental rate data, we have derived a predictive correlation for the site-specific H-abstraction at 298 K for substituted hydrocarbons.[28,29] Note that the existence of such a predictive correlation does not necessarily imply causality.[30,31] Given a C−H bond strength, *D*, in kcal/mol, calculated at the B3LYP-DFT/6-31G(d,p) level of theory, the site-specific H-abstraction rate can be predicted within approximately a factor of 2 with the following equation:

$$\log[k_{hyp}(298\text{ K})] = -0.00328D^2 + 0.3869D - 19.392 \quad \text{(v)}$$

for hydrogen atom abstraction where the product radical is stabilized only by hyperconjugation. For product radicals also stabilized by resonance delocalization of the radical electron other formulas apply, differing mainly in the size of the last constant for different types of resonances. The correlation is derived from experimental rate data and therefore already includes effects of H-bonding and tunneling and variational effects known to strongly affect the reactions of oxygenates with OH.[22,32,33] B3LYP-DFT/6-31G(d,p) and B3LYP-DFT/6-311+G-(2d,p) calculations show a marked increase of about 2.25 kcal/mol in the C(O)−H bond strength upon hydroxy substitution of the $-CH_3$ group in acetaldehyde. Applying the predictive correlation using these bond strengths, we obtain aldehydic H-abstraction rate coefficients of 2.0×10^{-11} cm^3 molecule^{-1} s^{-1} for acetaldehyde and 7.4×10^{-12} cm^3 molecule^{-1} s^{-1} for glycolaldehyde, in good agreement with both the absolute and the relative site-specific rate coefficients derived from the experimental total rate coefficient and product distribution. The reason for the increased difficulty in abstracting the aldehydic H-atom can perhaps best be illustrated by a population analysis mapping the charge distribution in the molecule. We thus used the CHelpG scheme[34] for matching charges to the electrostatic potential. In acetaldehyde, the carbon in the $-CH_3$ group is still negatively charged (−0.24) and can transfer some of its excess electrons to the carbonyl oxygen when the aldehydic hydrogen becomes unavailable as an electron donor for the carbonyl oxygen after abstraction. In contrast, the carbon in the $-CH_2$-OH group in glycolaldehyde is already positively charged (+0.31), donating its electrons to the oxygen in the hydroxy group; the $-CH_2OH$ group is less suited than a $-CH_3$ group to adjust the electron distribution toward the electronegative carbonyl oxygen after abstraction of the aldehydic hydrogen. Hence, the presence of two oxygen atoms in the small, hydrogen-poor hydroxy-substituted aldehyde is the main reason for the slowdown of the abstraction rate. All quantum chemical calculations were performed using the Gaussian-03 quantum chemical package.[35]

Quantum chemical calculations with canonical variational transition state theory calculations (CVT−SCT) including small-curvature tunneling corrections[22] show abstraction of the aldehydic H to be dominant, with a 90% contribution in the total rate coefficient at 298 K, corresponding to $k_{1a} = 6.5 \times 10^{-12}$ cm^3 molecule^{-1} s^{-1}, in good agreement with the considerations above. In contrast, variational TST calculations with multidimensional tunneling corrections (VTST−MT)[36] predict that abstraction of the aldehydic hydrogen is a less important channel, with 39% contribution at room temperatures, and $k_{1a} = 1.19 \times 10^{-11}$ cm^3 molecule^{-1} s^{-1} and a total rate coefficient $k_1 = 3.8 \times 10^{-11}$ cm^3 molecule^{-1} s^{-1}, which is nearly 5 times higher than measured in this work.

Virtually no site-specific data are available on H-abstraction with α-hydroxy-*β*-carbonyl substituents. It is well-known that α-hydroxy substitution increases the rate coefficient significantly (e.g., ethanol versus ethane),[10] in agreement with the lowering of the calculated C−H bond strengths. This supports a higher H-abstraction rate coefficient for the $-CH_2OH$ methylene hydrogens in glycolaldehyde, $k_{1b}(298\text{ K}) = 8 \times 10^{-13}$ cm^3 molecule^{-1} s^{-1} per hydrogen, compared to $-CH_3$ hydrogens in acetaldehyde (2.5×10^{-13} cm^3 molecule^{-1} s^{-1} per hydrogen) and acetone (3×10^{-14} cm^3 molecule^{-1} s^{-1} per hydrogen).

CVT−SCT calculations by Galano et al.[22] predicted a 10% contribution in the total rate coefficient for R1b at 298 K, corresponding to $k_{1b} = 7.4 \times 10^{-13}$ cm^3 molecule^{-1} s^{-1}, slightly below the value of k_{1b} derived from the experimental data. These authors also find the importance of channel (R1b) moderately increasing with increasing temperatures to, for example, 20% at 500 K. The VTST−MT calculations of Ochando-Pardo et al.[36] predict however that abstraction of the $-CH_2OH$ methylene hydrogens is dominant, with a 60% contribution at room temperatures, resulting in a value of $k_{1b} = 2.33 \times 10^{-11}$ cm^3 molecule^{-1} s^{-1}. This value is much higher than the total rate coefficient measured experimentally in this study.

3.3.2. Temperature and Pressure Dependence of k_1. The experimental data shows, within its statistical uncertainty of about 10%, a temperature-independent rate coefficient of 8×10^{-12} cm^3 molecule^{-1} s^{-1} over the temperature range considered, 240−362 K. The CVT−SCT calculations by Galano et al.[22] find two reaction ensembles with different behavior: a linear, negative T-dependence for reactions starting from reactants or reactant complexes with the internal H-bond of glycolaldehyde intact and a concavely curved T-dependence going through a maximum at 280 K for conformers where the $CH_2OH\cdots O{=}C$ intramolecular H-bond is absent. Summing the contributions of these reaction groups based on their relative (T-dependent) populations leads to a negative overall T-dependence. At about 285 K, the predicted rate coefficient matches the experimental $k_1 = 8 \times 10^{-12}$ cm^3 molecule^{-1} s^{-1}. Over the experimental temperature range of this work, the predicted rate coefficients change by a factor of 2.7, well beyond the experimental scatter, and such a variation in reaction rate should have been experimentally observed. VTST−MT calculations by Ochando-Pardo et al.[36] show a similar negative T-dependence for 100 <

$T < 350$ K. There is a clear discrepancy between the observed T-dependence and the available theoretical studies.

The layout of the potential energy surface[22] of the HO + glycolaldehyde reaction is similar to that of other HO + oxygenate reactions,[13,32,37,38] and the general behavior of $k(T)$ for these systems with an initial pre-reactive H-bonded complex formation followed by a H-abstraction TS is well documented. If the barrier to H-abstraction is sufficiently higher than the energy of the reactants, one finds a positive T-dependence except at the lowest of temperatures (due to tunneling); HO + acetone is a typical example. We have shown recently that virtually no pressure dependence is expected for such a system.[39] If the barrier to H-abstraction is below the energy of the reactants, the increasing importance of redissociation at increasing temperature will result in a negative temperature dependence of the overall rate coefficient, further enhanced by variational and tunneling effects; for example, the HO + acetaldehyde system has these properties. For these latter systems, one expects a clear pressure dependence.[39] We performed exploratory RRKM-Master Equation analysis on a template system using typical molecular parameters as found in quantum chemical studies to examine the behavior of the temperature dependence in between these distinct cases. We found that specific intermediate barrier heights slightly above the energy of the free reactants can generate an overall temperature-independent behavior over a fairly wide temperature range, similar to that measured for the title reaction. For the set of data we used, we found less than 1% change in the overall $k(T)$ between 300 and 500 K, and only 6% change between 250 and 750 K. Beyond these temperature limits, the rate coefficient again showed a clear temperature dependence. The barrier height needs to be within a fairly tight margin to generate the T-independent $k(T)$; varying the barrier height with 0.25 to 0.5 kcal/mol down or up generates smooth negative or positive T-dependences for $k(T)$, respectively, in agreement with the available data on other HO + oxygenate reactions. The transition state tightness for H-abstraction relative to initial complex-formation affects the required barrier height as well as the width of the T-range where T-dependence is negligible; variational and tunneling effects in the respective TSs likewise influence the needed barrier height and the extent of the observed effect. For all cases examined, we found no pressure dependence.

From these exploratory RRKM-ME calculations, we conclude that there is a distinct possibility that the barrier height for the glycolaldehyde + OH reaction is located in the small energy region where negative- and positive-temperature dependencies cancel out, resulting in a nearly T-independent $k(T)$. The observed lack of pressure dependence is also in agreement with our theoretical expectations for systems with such barrier heights and suggests that the barriers to H-abstraction cannot be significantly below the energy of the free reactants. The available theoretical kinetic results on glycolaldehyde + OH are in disagreement with the experimental data, showing a negative temperature dependence.[22,36] This suggests an underestimated barrier height, although the existence of multiple reaction channels and a clear impact of variational and tunneling effects makes it hard to estimate which parameter change is needed to bring theory and experiment in agreement. Further experimental work extending the temperature range, combined with theoretical work exploring the detailed impact of specific parameters in the models, is needed to address the current discrepancies.

3.1. Quantum Yield for HO Formation in the 248 nm Photolysis of $HOCH_2CHO$. As part of our kinetic study of R1, the photolysis of $HOCH_2CHO$ at 248 nm was used as the HO source. To characterize this source, we conducted experiments to determine the quantum yield of HO formation from $HOCH_2CHO$ photolysis relative to HO formation from HNO_3 photolysis at the same wavelength. The experiments (at a total pressure of 60 Torr He) were carried out back-to-back and the initial HO signal from photolysis of a known concentration of $HOCH_2CHO$ was compared to the HO signal from photolysis of a known concentration of HNO_3 at the same wavelength and at the same laser fluence (±3%). The initial HO signal were obtained by kinetic analysis of HO decays to derive the signal at $t = 0$. The relative signal heights are given by

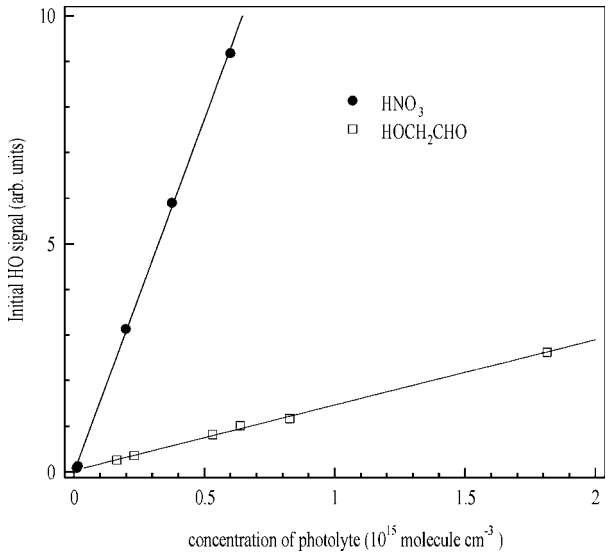

Figure 8. Plots of initial HO signal obtained in the photolysis of either $HOCH_2CHO$ or HNO_3 at 248 nm.

$$\frac{\text{signal(GLY)}}{\text{signal(HNO}_3\text{)}} = \frac{E_1 F_1 \Phi_{\text{GLY}} [\text{HOCH}_2\text{CHO}] \sigma^{248}_{\text{GLY}}}{E_2 F_2 \Phi_{\text{HNO}_3} [\text{HNO}_3] \sigma^{248}_{\text{HNO}_3}} \quad \text{(vi)}$$

where signal(GLY) and signal(HNO_3) are the initial HO signal from photolysis of $HOCH_2CHO$ or HNO_3, respectively, E_1 and E_2 are the laser fluences, and F_1 and F_2 are HO detection efficiencies and depend on several experimental parameters such as beam and optical geometries, dye laser intensity, photomultiplier settings etc. Φ_{GLY} and Φ_{HNO_3} are the primary quantum yields for HO formation from $HOCH_2CHO$ and HNO_3, respectively, $\sigma^{248}_{\text{GLY}}$and $\sigma^{248}_{\text{HNO}_3}$ are the absorption cross-sections of $HOCH_2CHO$ and HNO_3 at 248 nm. As the laser output (E) was stable to ≈2−3% during back-to-back experiments, and the detection sensitivity (F) does not change as long as HNO_3 and $HOCH_2CHO$ do not significantly quench the HO LIF signal, eq (vi) can be rearranged to

$$\frac{\text{signal(GLY)}/[\text{HOCH}_2\text{CHO}]}{\text{signal(HNO}_3\text{)}/[\text{HNO}_3]} = \frac{\Phi_{\text{GLY}} \sigma^{248}_{\text{GLY}}}{\Phi_{\text{HNO}_3} \cdot \sigma^{248}_{\text{HNO}_3}} \quad \text{(vii)}$$

The parameters on the left-hand side of the equation are derived from the slopes of a plot of initial signal versus the concentration of the photolyte as shown in Figure 8. The concentrations of $HOCH_2CHO$ and HNO_3 were measured at 184.9 nm in the 43.8 cm absorption cell, using cross-sections of $\sigma^{184.9}_{\text{GLY}} = 3.85 \times 10^{-18}$ cm^2 molecule^{-1} from this study and $\sigma^{184.9}_{\text{HNO}_3} = 1.84 \times 10^{-17}$ cm^2 molecule^{-1} from a separate study in this laboratory.[40]

Using $\sigma^{248}_{GLY} = 2.41 \times 10^{-20}$ cm^2 molecule^{-1} (taken from Magneron et al.[9]), $\sigma^{248}_{HNO_3} = 2.00 \times 10^{-20}$ cm^2 molecule^{-1} (taken from Burkholder et al.[41] and $\Phi^{248}_{HNO3} = 0.95$ (taken from Turnipseed et al.[42]), we derive a value of $\Phi^{248}_{GLY} = (7.0 \pm 1.5) \times 10^{-2}$. The errors on the quantum yield are obtained by propagating estimated errors of ≈5% on the absorption cross-section of HNO_3 and $HOCH_2CHO$ at 248 nm and 10% errors in [HNO_3], [$HOCH_2CHO$], and $\Phi^{248}_{HNO_3}$. By comparison, the statistical error on the gradients of Figure 8 is negligible.

The results obtained indicate a minor (7%) channel to form HO in the 248 nm photolysis of $HOCH_2CHO$. Other possible dissociation channels and, where appropriate, their approximate thermodynamic, threshold wavelengths are given below (note that reaction R2c is approximately thermoneutral):

$$HOCH_2CHO + h\nu \rightarrow HO + CH_2CHO\ (329\ nm) \quad (R2a)$$

$$\rightarrow CH_2OH + HCO\ (351\ nm) \quad (R2b)$$

$$\rightarrow CH_3OH + CO \quad (R2c)$$

$$\rightarrow H + HOCH_2CO\ (318\ nm) \quad (R2d)$$

The wavelength thresholds were calculated from evaluated heats of formation[10] for all species except for ΔH_f ($HOCH_2CHO$) = −316 kJ mol^{-1} and ΔH_f ($HOCH_2CO$) = −158 kJ mol^{-1}, which were taken from Espinosa-García and Dóbé.[43] Clearly, all channels are accessible at a photolysis wavelength of 248 nm.

A low yield in channel (R2a) is consistent with the indirect observations of Magneron et al.[9] who found evidence for HO formation in the low intensity, broadband (275−380 nm, or sunlight) CW photolysis of $HOCH_2CHO$ but who did not report a quantum yield. It is also consistent with the observations of Bacher et al.[6] who concluded that a photolytic source of HO was present in their chemical system, but which was assigned to an unknown secondary process. Although direct comparison is not justified owing to the use of different photolysis wavelengths and pressures, the result is consistent with the findings of Bacher et al.[6] and Magneron et al.[9] that the major photodissociation channel (65−80%) at UV wavelengths is formation of HCO and $HOCH_2$ via C−C bond breaking. A yield of 10% for channel R2c was found by Magneron et al.[9]

4. Conclusions and Atmospheric Implications

Rate coefficients for the reaction of HO with $HOCH_2CHO$ were, for the first time, determined over a range of temperatures. The overall rate coefficient from this work is adequately described by $k_1(240-362\ K) = (8.0 \pm 0.8) \times 10^{-12}$ cm^3 molecule^{-1} s^{-1}. The available theoretical data support a rate coefficient for HO + glycolaldehyde that is lower than for HO + acetaldehyde, with a clear dominance of the abstraction of the aldehydic hydrogen. The lack of a clear temperature dependence of the rate coefficient $k_1(T)$ over the 240−362 K temperature range can be explained by a H-abstraction transition state that is slightly higher in energy than the reactants, combined with tunneling effects.

For the purpose of atmospheric modeling, a value of $k_1 = 8.0 \times 10^{-12}$ cm^3 molecule^{-1} s^{-1} can be considered appropriate for most temperatures encountered in the troposphere. When combined with an estimated, diurnally averaged global HO concentration of ≈1×10^6 molecule cm^{-3}, we may calculate a atmospheric lifetime with respect to reaction R1 of ≈35 h. This is a factor of ≈2 shorter than the photolytic lifetime[6] and thus represents the major loss process.

Product studies and theoretical calculations have indicated that the major initial organic reaction products are the $HOCH_2CO$ radical (80%) and the HOCHCHO radical (20%). Reactions of these organic radicals with O_2 and further reactions of the peroxy and alkoxy radicals subsequently formed lead to the formation of CO, CO_2, HCHO, HC(O)CH(O), and HO_2. As both HCHO and HC(O)CH(O) are photodissociated efficiently to form HO_2 in the presence of O_2, the reaction of HO with $HOCH_2CHO$ ultimately results in the *net* formation of ≈1 HO*x* per $HOCH_2CHO$ lost. By comparison, the net HO*x* production in the photolysis of $HOCH_2CHO$ is 2.75 per $HOCH_2CHO$ lost if we consider only formation of HCO and CH_2OH (R2b). Thus, in terms of HO*x* production and taking the relative lifetimes into account, the HO and photolysis loss channels may be regarded as roughly equivalent.

Acknowledgment. The authors acknowledge financial support from the EU within the Energy, Environment and Sustainable Development program (EVK2-CT2001-00099, UTOPIHAN-ACT). L.V. is a postdoctoral research fellow of the FWO-Vlaanderen. R.K. carried out this research within the International Max-Planck Research School (IMPRS) in part fulfilment of her PhD at the Johannes Gutenberg Universität in Mainz.

References and Notes

(1) Guenther, A.; Hewitt, C. N.; Erickson, D.; Fall, R.; Geron, C.; Graedel, T.; Harley, P.; Klinger, L.; Lerdau, M.; McKay, W. A.; Pierce, T.; Scholes, B.; Steinbrecher, R.; Tallamraju, R.; Taylor, J.; Zimmerman, P. *J. Geophys. Res.* **1995**, *100*, 8873.

(2) Orlando, J. J.; Tyndall, G. S.; Bilde, M.; Ferronato, C.; Wallington, T. J.; Vereecken, L.; Peeters, J. *J. Phys. Chem. A* **1998**, *102*, 8116.

(3) Lee, Y. N.; Zhou, X.; Kleinman, L. I.; Nunnermacker, L. J.; Springston, S. R.; Daum, P. H.; Newman, L.; Keigley, W. G.; Holdren, M. W.; Spicer, C. W.; Young, V.; Fu, B.; Parrish, D. D.; Holloway, J.; Williams, J.; Roberts, J. M.; Ryerson, T. B.; Fehsenfeld, F. C. *J. Geophys. Res.* **1998**, *103*, 22449.

(4) Yokelson, R. J.; Susott, R.; Ward, D. E.; Reardon, J.; Griffith, D. W. T. *J. Geophys. Res.* **1997**, *102*, 18865.

(5) Williams, J.; Poschl, U.; Crutzen, P. J.; Hansel, A.; Holzinger, R.; Warneke, C.; Lindinger, W.; Lelieveld, J. *J. Atmos. Chem.* **2001**, *38*, 133.

(6) Bacher, C.; Tyndall, G. S.; Orlando, J. J. *J. Atmos. Chem.* **2001**, *39*, 171.

(7) Niki, H.; Maker, P. D.; Savage, C. M.; Hurley, M. D. *J. Phys. Chem.* **1987**, *91*, 2174.

(8) Baker, J.; Arey, J.; Atkinson, R. *J. Phys. Chem. A* **2004**, *108*, 7032.

(9) Magneron, I.; Mellouki, A.; Le Bras, G.; Moortgat, G. K.; Horowitz, A.; Wirtz, K. *J. Phys. Chem. A* **2005**, *109*, 4552.

(10) Atkinson, R.; Baulch, D. L.; Cox, R. A.; Crowley, J. N.; Hampson, R. F.; Hynes, R. G.; Jenkin, M. E.; Kerr, J. A.; Rossi, M. J.; Troe, J. IUPAC Subcommittee for gas kinetic data evaluation. Evaluated kinetic data. http://www.iupac-kinetic.ch.cam.ac.uk/, 2006.

(11) Wollenhaupt, M.; Carl, S. A.; Horowitz, A.; Crowley, J. N. *J. Phys. Chem. A* **2000**, *104*, 2695.

(12) Sivakumaran, V.; Crowley, J. N. *Phys. Chem. Chem. Phys.* **2003**, *5*, 106.

(13) Dillon, T. J.; Horowitz, A.; Hölscher, D.; Crowley, J. N. *Phys. Chem. Chem. Phys.* **2006**, *8*, 236.

(14) Baulch, D. L.; Cobos, C. J.; Cox, R. A.; Esser, C.; Frank, P.; Just, T.; Kerr, J. A.; Pilling, M. J.; Troe, J.; Walker, R. W.; Warnatz, J. *J. Phys. Chem. Ref. Data* **1992**, *21*, 411.

(15) Rensberger, K. J.; Jeffries, J. B.; Crosley, D. R. *J. Chem. Phys.* **1989**, *90*, 2174.

(16) Hancock, G.; Morrison, M.; Saunders, M. *J. Photochem. Photobio., A* **2005**, *176*, 191.

(17) Dillon, T. J.; Hölscher, D.; Sivakumaran, V.; Horowitz, A.; Crowley, J. N. *Phys. Chem. Chem. Phys.* **2005**, *7*, 349.

(18) Gierczak, T.; Talukdar, R. K.; Herdon, S.; Vaghjiani, G. L.; Ravishankara, A. R. *J. Phys. Chem.* **1997**, *101*, 3125.

(19) Paraskevopoulos, G.; Nip, W. S. *Can. J. Chem.* **1980**, *58*, 2146.

(20) Méreau, R.; Rayez, M. T.; Rayez, J. C.; Caralp, F.; Lesclaux, R. *Phys. Chem. Chem. Phys.* **2001**, *3*, 4712.

(21) Butkovskaya, N. I.; Pouvesle, N.; Kukui, A.; Le Bras, G. *J. Phys. Chem. A* **2006**, *110*, 13492.

(22) Galano, A.; Alvarez-Idaboy, J. R.; Ruiz-Santoy, M. E.; Vivier-Bunge, A. *J. Phys. Chem. A* **2005**, *109*, 169.

(23) Butkovskaya, N. I.; Kukui, A.; Le, Bras, G. *J. Phys. Chem. A* **2004**, *108*, 1160.

(24) Cameron, M.; Sivakumaran, V.; Dillon, T. J.; Crowley, J. N. *Phys. Chem. Chem. Phys.* **2002**, *4*, 3628.

(25) Peeters, J.; Vandenberk, S.; Piessens, E.; Pultau, V. *Chemosphere* **1999**, *38*, 1189.

(26) Vereecken, L.; Peeters, J. *Chem. Phys. Lett.* **2001**, *333*, 162.

(27) Vereecken, L.; Peeters, J. *Phys. Chem. Chem. Phys.* **2002**, *4*, 467.

(28) Peeters, J.; Vandenberk, S.; Pultau, V.; Boullart, W.; van Hoeymissen, J.; Fantechi, G.; Vereecken, L. Structure-activity relationships for some initiation and degradation pathways. ACCENT Symposium on the Changing Chemical Nature of the Troposphere, Urbino, Italy, 2005.

(29) Vereecken, L.; Peeters, J., manuscript in preparation, 2006.

(30) Donahue, N. M. *J. Phys. Chem. A* **2001**, *105*, 1489.

(31) Rypkema, H. A.; Donahue, N. M.; Anderson, J. G. *J. Phys. Chem. A* **2001**, *105*, 1498.

(32) Smith, I. W. M.; Ravishankara, A. R. *J. Phys. Chem. A* **2002**, *106*, 4798.

(33) Masgrau, L.; González-Lafont, A.; Lluch, J. M. *J. Phys. Chem. A* **2002**, *106*, 11760.

(34) Breneman, C. M.; Wiberg, K. B. *J. Comput. Chem.* **1990**, *11*, 361.

(35) Frisch, M. J., et al. Gaussian 03 (version C.01); Gaussian Inc.: Wallingford, CT, 2004.

(36) Ochando-Pardo, M.; Nebot-Gil, I.; Gonzalez-Lafont, A.; Lluch, J. M. *J. Phys. Chem. A* **2004**, *108*, 5117.

(37) Vandenberk, S.; Vereecken, L.; Peeters, J. *Phys. Chem. Chem. Phys.* **2002**, *4*, 461.

(38) De Smedt, F.; Bui, X. V.; Nguyen, T. L.; Peeters, J.; Vereecken, L. *J. Phys. Chem. A* **2005**, *109*, 2401.

(39) Peeters, J.; Vereecken, L. Hydrogen abstractions by hydroxyl through H-bonded complexes: pressure dependence. International Symposium on Gas Kinetics, Orléans, France, July 22−27, 2006.

(40) Winkler, A. K. Laboruntersuchungen zur Wechselwirkung atmosphpärischer Spurengase mit Eisoberflächen. Ph.D. Thesis, Johannes Gutenberg-Universität, 2004.

(41) Burkholder, J. B.; Talukdar, R. K.; Ravishankara, A. R.; Solomon, S. *J. Geophys. Res.* **1993**, *98*, 22937.

(42) Turnipseed, A. A.; Vaghjiani, G. L.; Thompson, J. E.; Ravishankara, A. R. *J. Chem. Phys.* **1992**, *96*, 5887.

(43) Espinosa-Garcia, J.; Dobe, S. *J. Mol. Struct.-Theochem.* **2005**, *713*, 119.